Biological Psychiatry

Archival Report

Loss of *CNTNAP2* Alters Human Cortical Excitatory Neuron Differentiation and Neural Network Development

Frances St George-Hyslop, Moritz Haneklaus, Toomas Kivisild, and Frederick J. Livesey

ABSTRACT

BACKGROUND: Loss-of-function mutations in the contactin-associated protein-like 2 (*CNTNAP2*) gene are causal for neurodevelopmental disorders, including autism, schizophrenia, epilepsy, and intellectual disability. *CNTNAP2* encodes CASPR2, a single-pass transmembrane protein that belongs to the neurexin family of cell adhesion molecules. These proteins have a variety of functions in developing neurons, including connecting presynaptic and postsynaptic neurons, and mediating signaling across the synapse.

METHODS: To study the effect of loss of *CNTNAP2* function on human cerebral cortex development, and how this contributes to the pathogenesis of neurodevelopmental disorders, we generated human induced pluripotent stem cells from one neurotypical control donor null for full-length *CNTNAP2*, modeling cortical development from neurogenesis through to neural network formation in vitro.

RESULTS: *CNTNAP2* is particularly highly expressed in the first two populations of early-born excitatory cortical neurons, and loss of *CNTNAP2* shifted the relative proportions of these two neuronal types. Live imaging of excitatory neuronal growth showed that loss of *CNTNAP2* reduced neurite branching and overall neuronal complexity. At the network level, developing cortical excitatory networks null for *CNTNAP2* had complex changes in activity compared with isogenic controls: an initial period of relatively reduced activity compared with isogenic controls, followed by a lengthy period of hyperexcitability, and then a further switch to reduced activity.

CONCLUSIONS: Complete loss of *CNTNAP2* contributes to the pathogenesis of neurodevelopmental disorders through complex changes in several aspects of human cerebral cortex excitatory neuron development that culminate in aberrant neural network formation and function.

https://doi.org/10.1016/j.biopsych.2023.03.014

Neurodevelopmental disorders, including autism spectrum disorder and intellectual disability, are associated with altered brain development, leading to impairments in cognition, communication, and behavior (1). The causes of neurodevelopmental disorders are highly heterogeneous (1), hindering efforts to investigate them and develop effective treatments. However, recent genetic studies have highlighted the contribution of de novo mutations in single genes to the development of these conditions. Those studies have enabled the identification of specific biological pathways that are frequently dysregulated in neurodevelopmental disorders, including pathways associated with neuronal differentiation and synaptic function (2).

One such gene is contactin-associated protein-like 2 (*CNTNAP2*). Heterozygous *CNTNAP2* missense and loss-of-function (LOF) mutations are causal for several neurodevelopmental disorders, including autism spectrum disorder (3–21), intellectual disability (22–25), specific language impairment (26–33), and epilepsy (34–37). Homozygous LOF mutations cause the most severe phenotypes, indicating that *CNTNAP2* dosage is important for determining disease severity (9,13,16,38,39).

CNTNAP2 encodes a single-pass transmembrane protein, also known as CASPR2, which belongs to the neurexin family of cell adhesion molecules (40). While the precise molecular functions of CNTNAP2 remain poorly understood, neurexins serve a variety of functions in the developing central nervous system, including mediating synaptic signaling (41). Additionally, CNTNAP2 interacts with contactin-2 (CNTN2), forming a complex thought to be required for the clustering of voltage-gated potassium channels (42). *CNTNAP2* LOF mutations are proposed to contribute to neurodevelopmental disorders through alterations in synaptic transmission, neuronal connectivity, and/or network-level activity. Consistent with this, complete loss of *Cntnap2* in the developing mouse reduces neurite branching and dendritic spine density in cortical neurons (43–48).

To study how loss of *CNTNAP2* function contributes to the pathogenesis of neurodevelopmental disorders in the developing human forebrain, we used CRISPR (clustered regularly interspaced short palindromic repeats)–Cas9 to generate human *CNTNAP2*-null induced pluripotent stem cells (iPSCs) from one neurotypical control donor. We used this system to replay cortical development from neurogenesis to neural

SEE VIDEO CONTENT ONLINE

ISSN: 0006-3223

network formation (49,50). We find that loss of *CNTNAP2* significantly alters human cortical excitatory neuron development, indicating that the pathogenesis of neurodevelopmental disorders due to *CNTNAP2* LOF begins early in development.

METHODS AND MATERIALS

Full experimental methods are given in Supplemental Methods. A summary of the number of cell lines and replicates used in each experiment is reported in Table S7.

Human PSC Culture and Neural Differentiation

PSCs were differentiated to cerebral cortex progenitor cells, according to our reported methods (49).

CRISPR-Cas9 Genome Engineering

CRISPR gene targeting of exon 3 of *CNTNAP2* in NDC1.2 iPSCs [control, male, 86 years, Caucasian (51)] was performed using methods adapted from Bruntraeger *et al.* (52).

Single-Cell Messenger RNA Sequencing

CNTNAP2 null and isogenic control PSC-derived cortical differentiations, 50 days after neural induction (D50), were dissociated using the Papain Dissociation System and multiplexed using cell hashing antibodies, as previously described (53). Single-cell sequencing was performed using the 10x Genomics Single Cell 3′ kit version 2, and count matrices were analyzed using the Seurat (version 4; Paul Hoffman, Satija Laboratory and Collaborators) package. Differential expression between null and control samples was performed using DESeq2 (Bioconductor) (54) on pseudobulk-aggregated counts.

Neurite Length and Branching Measurement

CNTNAP2 null and isogenic control neurons were sparsely nucleofected with a fluorescent construct at D50 using an Amaxa 4D (Rensselaer Polytechnic Institute) nucleofector. Cultures were subsequently imaged on an Opera Phenix confocal microscope every 3 to 6 days until D61 or D66. Following image acquisition, neurite length and branching were measured with NeuronStudio (Lumitos AG) software (55).

Calcium Imaging and Multielectrode Array Analyses

Calcium imaging was conducted using the Incucyte S3 (Thermo Fisher Scientific). For multielectrode array (MEA) analyses, activity was recorded on a Maestro Pro MEA system, using the accompanying Axis Navigator software.

RESULTS

CNTNAP2 Is Highly Expressed in Differentiating Cortical Excitatory Neurons In Vitro and In Vivo

To determine the developmental expression of *CNTNAP2*, we measured *CNTNAP2* messenger RNA (mRNA) and protein throughout cortical differentiation from iPSCs. For this, we used our established method to differentiate human iPSCs to cerebral cortex neural progenitor cells and glutamatergic excitatory cortical neurons (Figure 1A) (49,50,56). With this method, neurons are generated in the same temporal order and over a comparable timeframe as observed in utero (49,50,56). iPSC-derived neurons also display similar gene expression profiles to their primary counterparts (Figure 1B; Figure S1) (49,50,57).

There are 4 predicted protein-coding isoforms of *CNTNAP2* (58–60), including the canonical full-length transcript referred to as CNTNAP2-201 (Figure 1C). During cerebral cortex development there is clear evidence for the expression of CNTNAP2-201 as well as a short isoform, CNTNAP2-203, which is located at the 3′ end of the locus and encodes a predicted 12-kDa protein (Figure S2). Because the majority of known disease-associated mutations affect only the full-length transcript, we focused the functional studies reported here on that *CNTNAP2* isoform (38,61).

CNTNAP2 expression was measured by quantitative reverse transcriptase polymerase chain reaction at 4 stages of the cortical differentiation process: 1) PSCs (i.e., pre-differentiation), 2) cortical neural progenitor cells (D30), 3) early-born deep layer neurons (D50), and 4) late-born deep layer neurons (D80). The latter time point also includes the period of maturation of deep layer neurons that would have been generated over the previous 30 days. Full-length *CNTNAP2* mRNA levels significantly increased during the cortical differentiation process, with no expression detected in iPSCs (one-way repeated-measures analysis of variance [ANOVA]: $F_{3,24} = 167.9$, $p = 3.1 \times 10^{-16}$) (Figure 1D). *CNTNAP2* mRNA was first detected at D30, when most cells are cortical progenitor cells and was significantly more highly expressed than iPSCs ($p = 1.0 \times 10^{-3}$ for iPSC vs. D30). Expression of *CNTNAP2* significantly increased between D50 and D80 ($p = 4.1 \times 10^{-5}$ for D50 vs. D80). Therefore, *CNTNAP2* is most highly expressed in postmitotic neurons, increasing over time, and is also expressed in neural progenitor cells but at a significantly lower level.

Comparison of the in vitro time course of *CNTNAP2* expression with a publicly available RNA sequencing (RNA-Seq) dataset of primary fetal cortex (62) indicated that in vivo developmental expression follows equivalent temporal and cell type patterns. Both long and short *CNTNAP2* isoforms are present as early as postconception week 8 (PCW 8) in human prefrontal cortex (Figure 1E) (earlier data are not currently available). Expression then rises until PCW 12, which would match the increased *CNTNAP2* expression between D50 to D80 in vitro. Cortical neurogenesis begins in human embryos around PCW 7 (63,64), thus the onset of *CNTNAP2* expression at PCW 8, and its subsequent increase, is consistent with most expression being in postmitotic neurons.

Expression of the long isoform of CNTNAP2 protein follows the same temporal progression during iPSC differentiation as its mRNA, first becoming detectable in cortical progenitor cells (D30) and increasing thereafter (ANOVA: $F_{3,9} = 55.8$, $p = 3.9 \times 10^{-6}$; pairwise t tests: $p = .008$ for iPSC vs. D50; $p = .03$ for D30 vs. D80) (Figure 1F). Immunofluorescence and confocal microscopy of iPSC-derived neurons found that CNTNAP2 is enriched in discrete puncta along axons, dendrites, and neuronal cell bodies (Figure 1G). Puncta colocalized with both presynaptic (SYP^+) and postsynaptic markers ($PSD\text{-}95^+$), indicating that CNTNAP2 is present at the neuronal synapse, as previously reported in mice (48).

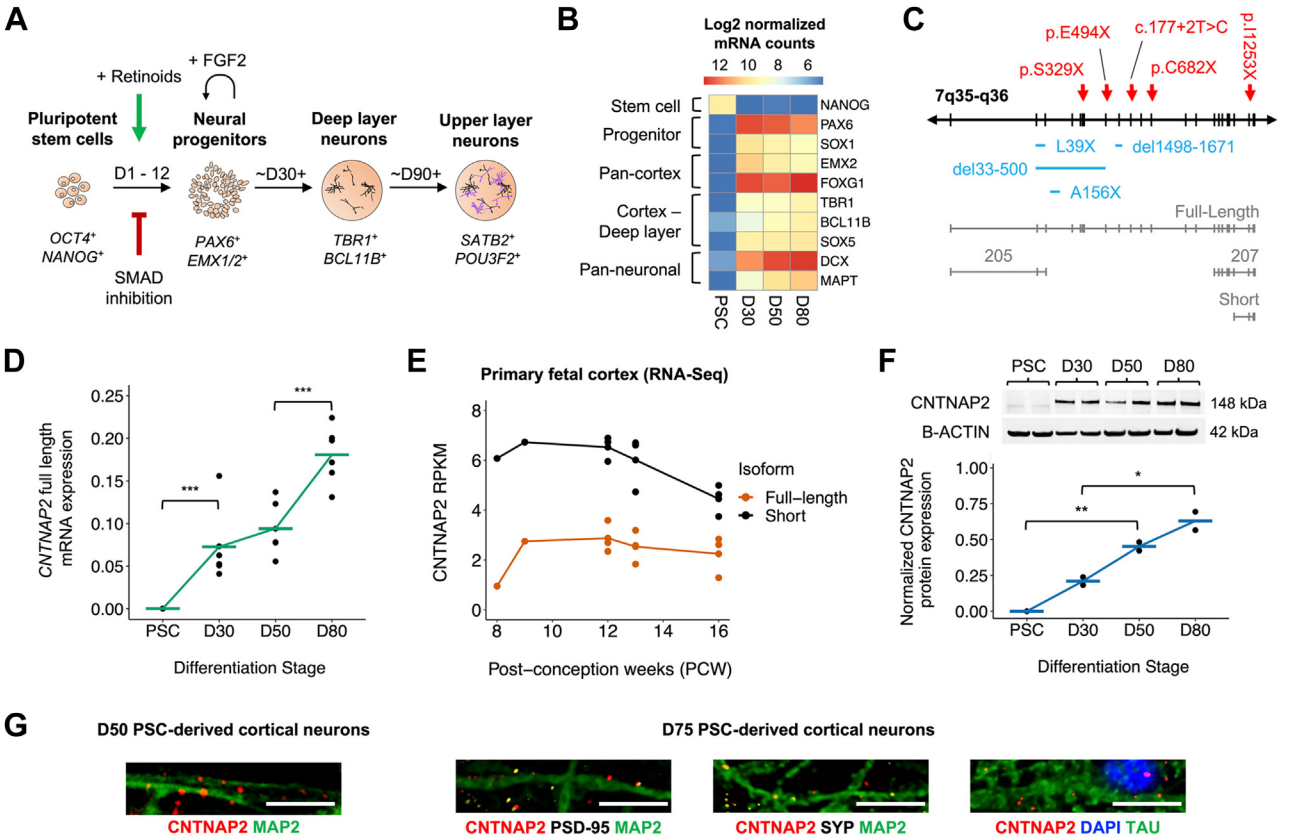

Figure 1. Temporal expression of *CNTNAP2* during early cerebral cortex development. **(A)** Diagram of the retinoid/dual-SMAD inhibition process used in this study for replaying cerebral cortex development from neural progenitor cells to excitatory cortical neuron differentiation and circuit formation. Examples of genes expressed in each stage of the process are shown in italics. **(B)** Efficient induction of cortical progenitor cells and cortical neurons from human iPSCs confirmed by the expression of key indicator genes in D30 progenitors and D50 to D80 neurons ($n = 3$ inductions). Pluripotency genes are downregulated, and progenitor/neuron-expressed genes are upregulated during the induction process, as measured with a custom Nanostring gene expression array (see Methods and Materials for details). **(C)** Diagram of known and predicted protein-coding isoforms of *CNTNAP2*: transcripts 201 (full-length), 203 (short), 205, and 207. Transcripts 201 and 203 are robustly expressed during cortical development. Notably, homozygous loss-of-function mutations predominantly overlap with the full-length isoform, as indicated (truncating mutations, red; microdeletions, blue). **(D)** The mRNA encoding the long isoform of *CNTNAP2* increases in expression during neurogenesis and cortical neuron differentiation. Expression of the full-length form of *CNTNAP2* was measured by quantitative reverse transcriptase polymerase chain reaction with primers targeting exons 3 and 4 and normalized to *RAB7A* ($n = 3$ inductions) (repeated-measures analysis of variance; post hoc paired *t* tests adjusted with Bonferroni correction). Expression was measured in iPSCs, cortical progenitor cells (D30) and 2 stages of neurogenesis and neuronal differentiation (D50 and D80). $^{*}p < .05$; $^{**}p < .01$; $^{***}p < .001$. Mean expression at each time point is shown in green. **(E)** The full-length and short isoforms of *CNTNAP2* are expressed in primary human fetal cortex and expression of full-length *CNTNAP2* increases between 8 and 9 PCW. Isoform-specific relative expression of *CNTNAP2* was derived from publicly available bulk RNA-Seq data of the human dorsolateral prefrontal cortex in the BrainSpan atlas. **(F)** CNTNAP2 protein levels increase over the period of cortical development from iPSCs, reflecting the temporal expression of the corresponding mRNA. Western blot of full-length CNTNAP2 protein and relative quantitation of CNTNAP2 levels normalized to β-actin are shown ($n = 2$ inductions) (same statistical tests as with quantitative reverse transcriptase polymerase chain reaction). $^{*}p < .05$, $^{**}p < .01$, $^{***}p < .001$. Mean expression at each time point is shown in blue. Example blot from one induction (cell line = AD2.1) is provided. **(G)** CNTNAP2 is expressed as puncta on axons and dendrites of D50 human excitatory cortical neurons. Confocal images of CNTNAP2 immunostaining (red) appears along dendrites (MAP2, green), axons (tau, green) and cell bodies (nuclei labeled with DAPI, blue). By D75, CNTNAP2 localizes to synapses, as shown by the overlap with PSD-95 and Synaptophysin (both yellow). Scale bar = 5 μm. iPSC, induced PSC; mRNA, messenger RNA; PCW, postconception week; PSC, pluripotent stem cell; RNA-Seq, RNA sequencing; RPKM, reads per kilobase, per million mapped reads.

Loss of Function of the Long Isoform of *CNTNAP2* Does Not Impair Directed Differentiation of Human iPSCs to Cortical Neurons

To generate human iPSCs with loss-of-function (LOF) alleles in *CNTNAP2*, a guide RNA was designed to disrupt the gene at exon 3 in the NDC1.2 cell line (Figure S3A) (52). Successful targeting was confirmed by MiSeq next generation sequencing (Illumina) and Sanger sequencing of genomic DNA. This sequencing revealed insertion of the stop codon in both alleles of edited iPSC clones (Figure S3B, C). Comparison of cell fate patterning between null and control inductions was performed using the Nanostring nCounter Sprint Profiler, using a custom-designed human brain development code set of 150 genes

described by Strano *et al.* (56). Results from this analysis showed that null and control cultures were not significantly different in composition (Welch's *t* test corrected for multiple testing: $p > .05$) (Figure S3D; Table S2). Finally, specific LOF of the long isoform of *CNTNAP2* was confirmed at the level of mRNA and protein in D50 cortical neurons by quantitative reverse transcriptase polymerase chain reaction and Western blot (Figure S3E, F).

To gain insights into both cell composition and cell type–specific gene expression changes as a consequence of *CNTNAP2* LOF during human cortical development, single-cell RNA-Seq (scRNA-Seq) was carried out on 2 independent cortical differentiations from *CNTNAP2* null and isogenic control iPSCs (Figure S4). Single-cell analyses were performed using the 10x Genomics platform at D50, a point of large-scale network formation (57) and high CNTNAP2 protein expression. A selection of cell type–associated marker genes (Figure S5) was used to identify clusters corresponding to 7 broad cell types, including cortical excitatory neurons and progenitors (Figure 2A, B).

We used the single-cell dataset to investigate cell type–specific expression of the long isoform of *CNTNAP2* in cortical development (Figure S6). Because the scRNA-Seq approach used here only detects the 3′ end of transcripts, which, in the case of *CNTNAP2* is shared by the long and short isoforms, it cannot distinguish between the different transcripts (58–60,65). However, quantitative reverse transcriptase polymerase chain reaction showed that targeting the 5′ exons of the gene specifically reduced full-length *CNTNAP2* expression (Figure S3E). Therefore, we examined differential expression of *CNTNAP2* between control and *CNTNAP2* null cell types, finding that cortical neurons were the only cell type in which total *CNTNAP2* expression was significantly reduced in null differentiations (Figure 2C). This suggests that the long form of *CNTNAP2* is primarily expressed in neurons. Notably, cortical neurons also exhibited the highest number of differentially expressed genes (Figure 2D), indicating that the loss of *CNTNAP2* directly leads to altered gene expression in those cells.

To investigate the effects of *CNTNAP2* LOF on cortical differentiation at single-cell resolution, the subset of cells that was identified as cortical progenitors and neurons was extracted for further analysis (4917 cells out of the total 11,941 analyzed). To assign predicted differentiation paths in an unbiased manner, we first ordered cells using a pseudotime algorithm (66), which identified a single trajectory from progenitor cell to differentiating neurons (Figure 2E, F).

Comparing gene expression between *CNTNAP2* null and isogenic control cortical neurons identified several mRNAs with large differences in gene expression (Figure 2G; Table S3), most notably, increased expression of calretinin (*CALB2*) and neurotensin (*NTS*) in *CNTNAP2* null neurons, and decreased expression of *LMO3*, *NEUROD2*, and *CSRP2*. Inspecting the expression of these genes along the pseudotime trajectory, *CALB2* and *NTS* are expressed in control neurons before *LMO3*, although this trend is less clear for *NEUROD2* and *CSRP2* (Figure 2H). In *CNTNAP2* null neurons, *CALB2* expression begins earlier than in controls, with *LMO3* delayed relative to controls.

Loss of *CNTNAP2* Results in Altered Differentiation of Cortical Neuron Subtypes

To further analyze the significance of the alterations in gene expression in postmitotic cortical neurons, the subset of cortical neurons in the dataset were extracted and reclustered (Figure 3A). Four clear populations were identified, representing differentiating neurons, early postmitotic neurons, and 2 well-separated populations of terminally differentiated neurons, referred to here as the late 1 and 2 groups (Figure S7; Table S4).

The 2 genes highly differentially expressed between *CNTNAP2* null and isogenic control neurons, *LMO3* and *CALB2*, mapped robustly onto the late 2 and late 1 clusters, respectively, as did *NEUROD2* and *NTS* (Figure 3B). This indicates that the differential expression between *CNTNAP2* null neurons and controls most likely reflects a change in the proportions of these 2 neuronal types. Consistent with this, we found a reduction in $LMO3^+$, late 2 neurons in *CNTNAP2* null compared with controls, and an accompanying increase in $CALB2^+$, late 1 neurons (Figure 3C, D). This increase was not due to simple experimental variation during cortical differentiation, because it was found in 2 independent cortical inductions from iPSCs.

The 2 cell types that show significant reductions in *CNTNAP2* expression in the null differentiations are the late 1 and late 2 populations, with the greatest reduction in expression observed in the $LMO3^+$/late 2 population (Figure 3E). In addition to changes in cell type composition, we also analyzed differential gene expression between *CNTNAP2* null and isogenic control $CALB2^+$/late 1 and $LMO3^+$/late 2 neurons (i.e., within each population) (Figure 3F, G; Table S5). For both populations, *CALB2* and *NTS* were highly upregulated in the *CNTNAP2* null, and *LMO3* was downregulated. Additionally, gene set enrichment analysis identified there was a significant downregulation of a set of genes that all encode elements of the cholesterol and fatty acid synthesis pathways, including *HMGCR* and *HMGCS1* (Table S6). In primary fetal cortex, these genes are most highly expressed in neurons of early and intermediate maturity, with expression reduced in late neurons (67). Thus, these data are consistent with an overproduction of early *CALB2*-expressing neurons and an underproduction of later differentiating $LMO3^+$ neurons.

Reduced Neurite Branching in Human *CNTNAP2* Null Cortical Neurons

Previous studies in mice null for *CNTNAP2* identified changes in neurite number and branching (43–45). Therefore, we investigated whether loss of *CNTNAP2* affects neurite outgrowth from human cortical excitatory neurons. We utilized 2 experimental approaches, comparing neurite outgrowth in 1) homogeneous cultures and 2) mixed cultures. In the homogeneous cultures, control and *CNTNAP2* null neurons were plated and maintained separately (Figure 4A). In the mixed cultures, control and *CNTNAP2* null neurons were labeled in different colors and cocultured at a 1:1 ratio. In addition to addressing cell autonomous effects, this second strategy also controls for variation in cellular environment. For imaging neurites, neurons were transfected with fluorescent expression

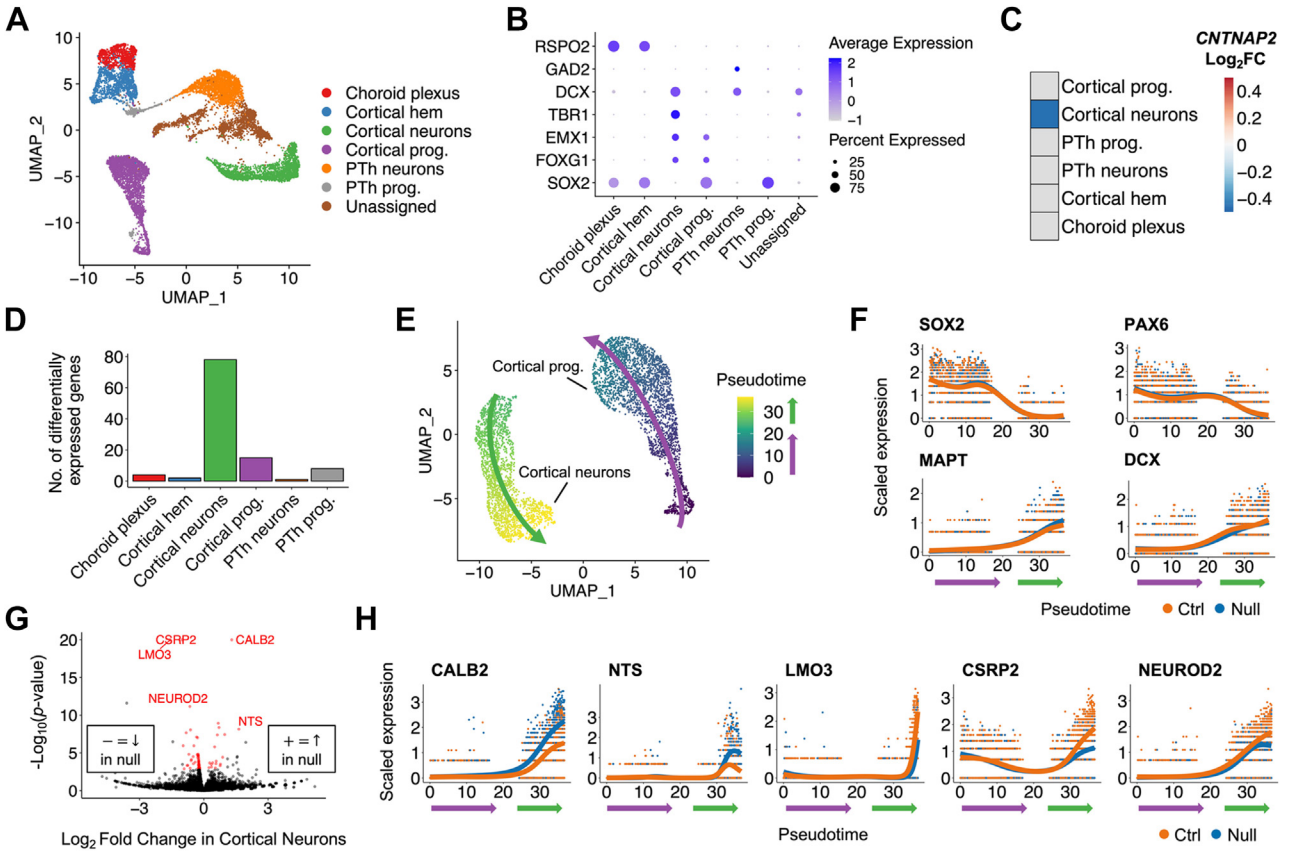

Figure 2. Loss of *CNTNAP2* primarily alters gene expression in cortical neurons. **(A)** Single-cell RNA sequencing data of D50 forebrain cultures derived from *CNTNAP2* null and isogenic control human induced pluripotent stem cells identified 6 major cell types (n = 2 null inductions, 2 control inductions, genetic background = NDC1.2). Data are represented as a UMAP projection of the 11,941 cells analyzed. **(B)** Expression of classifier genes used to assign cell type identities, including *SOX2* for progenitor cells and *DCX* for postmitotic neurons. Cortical progenitor cells and cortical neurons were further identified by the expression of *FOXG1* and *EMX1* as well as *TBR1*, for neurons only. *GAD2* identified inhibitory cells and *RSPO2* identified medial telencephalon (cortical hem and choroid plexus). **(C)** Full-length *CNTNAP2* is predominantly expressed by cortical neurons. Differential expression of *CNTNAP2* was used as a proxy for full-length expression, which is specifically reduced in the null lines as shown in **(D)**. The heatmap shows the $\log_2$FC between *CNTNAP2* null samples and isogenic controls. Comparisons that were not significant (adjusted p value $\geq$ .05) are shown in gray. **(D)** Cortical neurons show the highest number of differentially expressed genes, signifying that loss of full-length *CNTNAP2* in cortical neurons directly leads to altered gene expression. The number of genes shown includes only those passing statistical significance (adjusted p value $<$ .05). **(E)** Cortical development is represented by a single trajectory in D50 forebrain cultures. Trajectory was inferred by pseudotime ordering of cortical progenitor cells and cortical neurons within the dataset. UMAP plot shows cells colored by relative pseudotime value with cells early in cortical development in purple and cells latest in development in yellow. Arrows indicate the trajectory among cortical progenitor cells (purple) and cortical neurons (green). **(F)** Expression of genes with known progenitor cell and neuronal expression in human cortical development validate the inferred trajectory. Relative gene expression in cells of the cortical lineage is shown ordered by cortical pseudotime. The line represents the fit of a negative binomial generalized additive model for the indicated gene along pseudotime separately for cells from *CNTNAP2* null or isogenic control samples. Values from individual cells and fitted lines are colored by genotype. Genes regulating cortical progenitor cell maintenance (*SOX2* and *PAX6*) show the highest expression at the beginning of the trajectory, and genes known to increase with neuronal maturation (*MAPT* and *DCX*) show the highest expression toward the end. The expression patterns of these genes do not differ between *CNTNAP2* null and isogenic control samples. Arrows under the x axes indicate the pseudotime values associated with cortical progenitors (purple) and cortical neurons (green). **(G)** Differentially expressed genes between *CNTNAP2* null and control cortical neurons. The volcano plot shows the $\log_2$FC and associated p value for each gene, with genes passing statistical significance highlighted in red (adjusted p value $<$ .05) (78 genes). Genes with a negative $\log_2$FC have higher expression in control neurons and those with a positive FC have higher expression in null neurons. **(H)** Differentially expressed genes between *CNTNAP2* null and control cortical neurons show the highest expression toward the end of the cortical trajectory. Relative expression and generalized additive model-fitted lines for *CALB2* and *NTS* (higher expression in null neurons) as well as *LMO3*, *NEUROD2*, and *CSRP2* (higher expression in control neurons) is shown ordered by cortical pseudotime, as in **(F)**. $\log_2$FC, $\log_2$ fold change; prog., progenitor; PTh, prethalamus; UMAP, Uniform Manifold Approximation and Projection.

constructs at day 35, which birthdated the nucleofected neurons as a cohort. Randomly selected neurons were imaged live from ~D40 until ~D65, and neuron reconstruction software (55) was used to measure 3 parameters: neurite branching, neurite length, and total neuron length (Figure 4B). Example images of D60 neurons are provided in Figure 4C.

For mixed cultures, a significant reduction in the number of branches per neuron was detected in *CNTNAP2* null cells

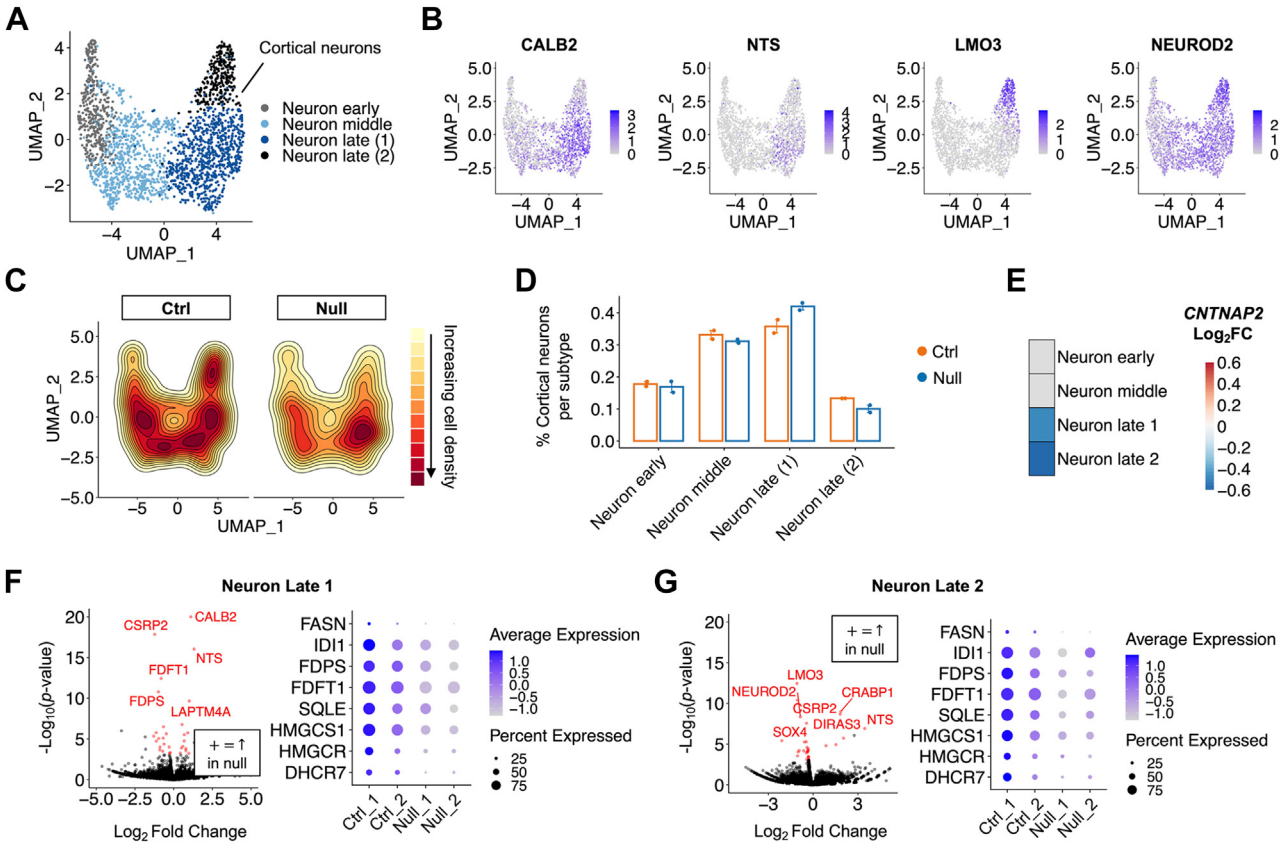

Figure 3. *CNTNAP2* loss of function alters the production of cortical neuron subtypes. **(A)** Subclustering of cortical neurons reveals 4 subpopulations that are separated by relative maturity, as defined by increasing expression of neuronal maturation genes (*MAPT* and *DCX*) and decreasing expression of progenitor-associated genes (*PAX6* and *EOMES*). UMAP projection shows cortical neurons colored by subpopulation. **(B)** The 2 genes most differentially expressed between *CNTNAP2* null and isogenic control neurons, *CALB2* and *LMO3*, separate late 1 and late 2 neuronal clusters, respectively, as do *NTS* and *NEUROD2*. UMAP projections of cortical neurons are colored by the relative expression of the indicated genes. **(C, D)** The relative proportion of the 2 most mature neuron subpopulations are shifted between *CNTNAP2* null and control samples. In **(C)** cell density is shown overlaid onto the UMAP projection of cortical neurons (separated by genotype). The density of *CALB2*$^+$, late 1 neurons is increased in the *CNTNAP2* null samples, while the density of *LMO3*$^+$, late 2 neurons is reduced. In **(D)** the percentage of all cortical neurons belonging to each subpopulation is plotted (separated by genotype). Error bars represent standard error of the mean. **(E)** Full-length *CNTNAP2* is expressed in the most mature neuronal populations (late 1 and 2). Differential expression of *CNTNAP2* was used as a proxy for full-length expression as in **(C)**. Log_2FC between *CNTNAP2* null and control samples in the indicated population is shown as a heatmap with comparisons not passing statistical significance (adjusted p value $\geq .05$) in gray. **(F, G)** Differential gene expression between *CNTNAP2* null and control samples in late 1 **(F)** and late 2 **(G)** cortical neurons. Volcano plots show the log_2FC and p value for each gene, with genes passing statistical significance (adjusted p value $< .05$) highlighted in red. In both late 1 and late 2 cortical neurons, *CALB2* and *NTS* were highly upregulated in the *CNTNAP2* null samples, while *LMO3* was downregulated. Additionally, downregulation of multiple genes belonging to the cholesterol and fatty acid synthesis pathways, including *SQLE, FDFT1, DHCR7, HMGCR*, and *HMGCS1*, was also observed in *CNTNAP2* null neurons from both late 1 and late 2 subtypes. Expression of example cholesterol and fatty acid synthesis genes in late 1 and late 2 neurons is shown as a dot plot separated by sample of origin. Dot color represents scaled expression levels and dot size the percentage of cells with nonzero expression. Ctrl, control; log_2FC, log_2 fold change; UMAP, Uniform Manifold Approximation and Projection.

(Figure 4D) (two-way repeated-measures ANOVA; separate cultures: $F_{1,17} = 0.79$, $p = .39$; mixed cultures: $F_{5,175} = 14.54$, $p = 6.51 \times 10^{-12}$). While ANOVA for separate cultures did not reach significance, post hoc comparisons did identify *CNTNAP2* null cells as having a significantly reduced number of branches at D55 ($p = .025$ after Bonferroni correction). Significant reductions were also found at D55, D60, and D66 in the mixed cultures (by both ANOVA and post hoc analyses) (post hoc: $p = .015$, $p = 5 \times 10^{-6}$, and $p = .041$, respectively).

For average neurite branch length, no significant difference was detected between control and *CNTNAP2* null neurons at any time point in the separate genotype experiment (Figure 4E) (two-way repeated-measures ANOVA: $F_{1,17} = 0.41$, $p = .53$). This was confirmed by post hoc analyses, in which $p > .05$ for all comparisons. In the mixed cultures, repeated-measures ANOVA also did not reach significance (ANOVA $F_{1,35} = 1.1$, $p = .3$). However, post hoc pairwise comparisons (corrected for multiple testing) did find *CNTNAP2* null neurons to have significantly increased branch length at D48 and D60 ($p = .017$ and $p = .006$).

Finally, *CNTNAP2* knockout did not affect total neuron length in genotype-specific cultures (Figure 4F) (two-way repeated-measures ANOVA: $F_{1,17} = 0.079$, $p = .78$, post hoc:

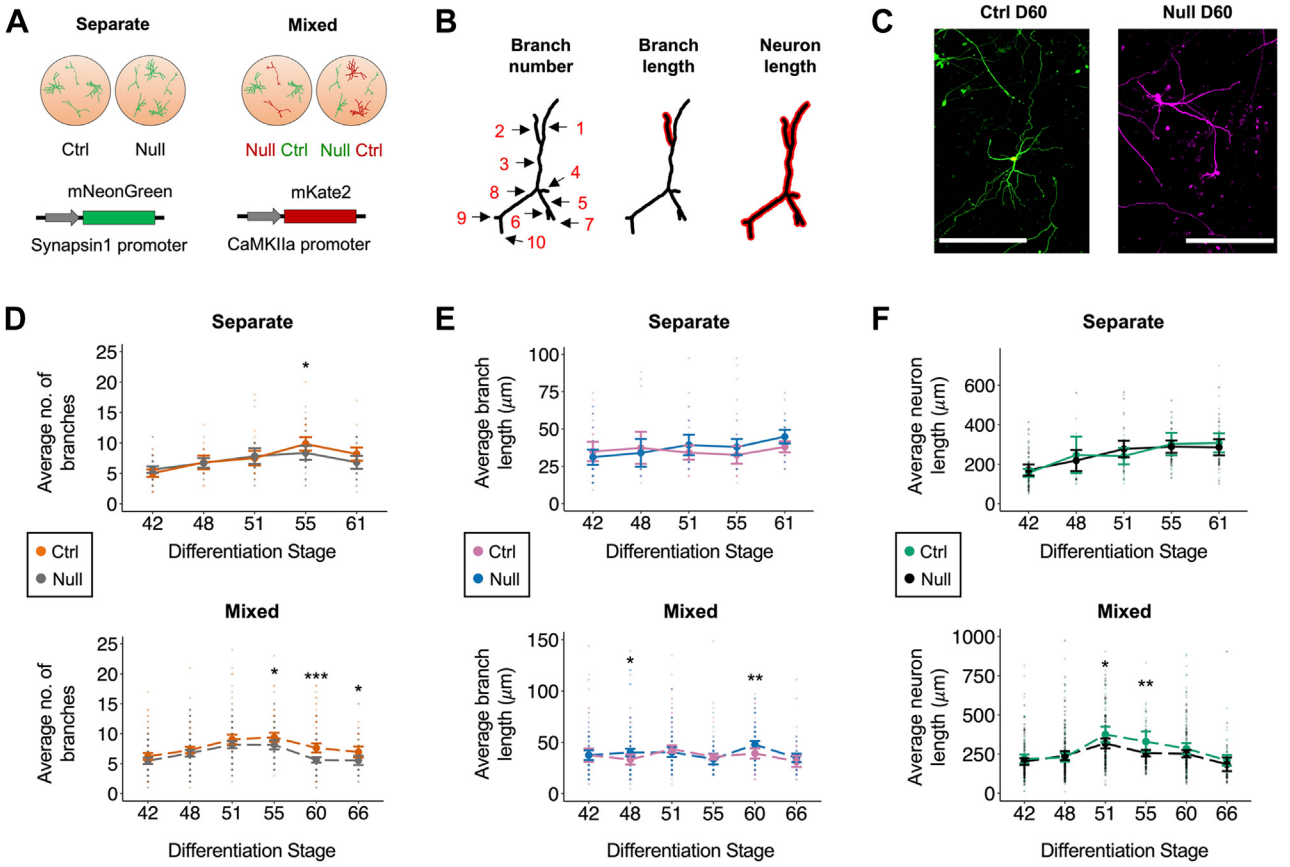

Figure 4. Loss of full-length *CNTNAP2* reduces neurite branching and overall neuronal complexity in a cell autonomous manner. **(A)** *CNTNAP2* null and isogenic control cultures were either plated into wells separately (i.e., by genotype) or mixed (cocultured). To facilitate the tracing of individual neurons, neurons of each genotype were nucleofected with different fluorescent reporters under the control of a neuron-specific promoter. For each mixed plating, 2 experiments were conducted with fluorescent proteins swapped between genotypes in the second iteration. **(B)** Three parameters of neurite outgrowth were measured: branch number, the sum of discrete segments composing a neuron; branch length, the distance from a branch point to a branch tip or to the next branch point; and total neuron length, the sum of all branch lengths. **(C)** Representative examples of labeled single *CNTNAP2* null and control neurons used as input for neurite analysis. Scale bar = 200 μm. **(D–F)** *CNTNAP2* null neurons have significantly reduced neuronal complexity. The number of branches **(D)**, average branch length **(E)**, and average total neuron length **(F)** were determined for *CNTNAP2* null and control neurons from cultures either plated individually by genotype or mixed. *CNTNAP2* null neurons showed significantly fewer branches per neuron, independent of plating type **(D)**. Branch length **(E)** was significantly increased in mixed cultures only, and neuron length was significantly decreased in mixed cultures. $^{*}p < .05$, $^{**}p < .01$, $^{***}p < .001$; repeated-measures analysis of variance; post hoc estimated marginal means analysis with Bonferroni correction; n = 648 control neurons, 662 null neurons from 2 inductions per genotype; error bars represent 95% confidence intervals. Both means (large dots) and individual data points (small dots) are plotted. CaMKII, calcium/calmodulin-dependent protein kinase II; Ctrl, control.

$p > .05$ for all). However, in mixed cultures, *CNTNAP2* null neurons had significantly reduced total length at D51 and D55 (two-way repeated-measures ANOVA: $F_{1,35} = 5.4$, $p = 2.60 \times 10^{-2}$; D51: $p = .019$; D55: $p = .0087$). Taken together, these findings indicate that *CNTNAP2* LOF reduces neurite branching, and thus dendritic arbor complexity, but has little effect on neurite branch length.

CNTNAP2 Loss of Function Alters Neuronal Activity in Developing Human Cortical Networks

Given the reduction observed in neurite branching, we measured neuronal activity to investigate whether this affected cortical neural network development. To measure network-level neuronal activity, we used 2 complementary but independent approaches, calcium imaging and MEAs (Figure 5A). Calcium imaging was performed by infecting D40 isogenic control and *CNTNAP2* null cultures with a lentivirus expressing a genetic calcium indicator (NeuroBurst Orange; Incucyte) (Supplemental Videos S1 [control] and S2 [null]). Confocal images of example cultures are provided in Figure 5B. Activity was subsequently recorded every 24 to 48 hours for 2 minutes until D105. A two-way ANOVA detected significant effects of culture age and *CNTNAP2* LOF on both the number of active objects and the average burst rate (Figure 5C) (active objects: $F_{39,560} = 297.4$, $p < .0001$; burst rate: $F_{39,560} = 68.21$, $p < .0001$). Notably, several other activity parameters also showed similar trends (Figure S8).

Out of the 40 time points examined, post hoc comparisons found that the majority had a significant

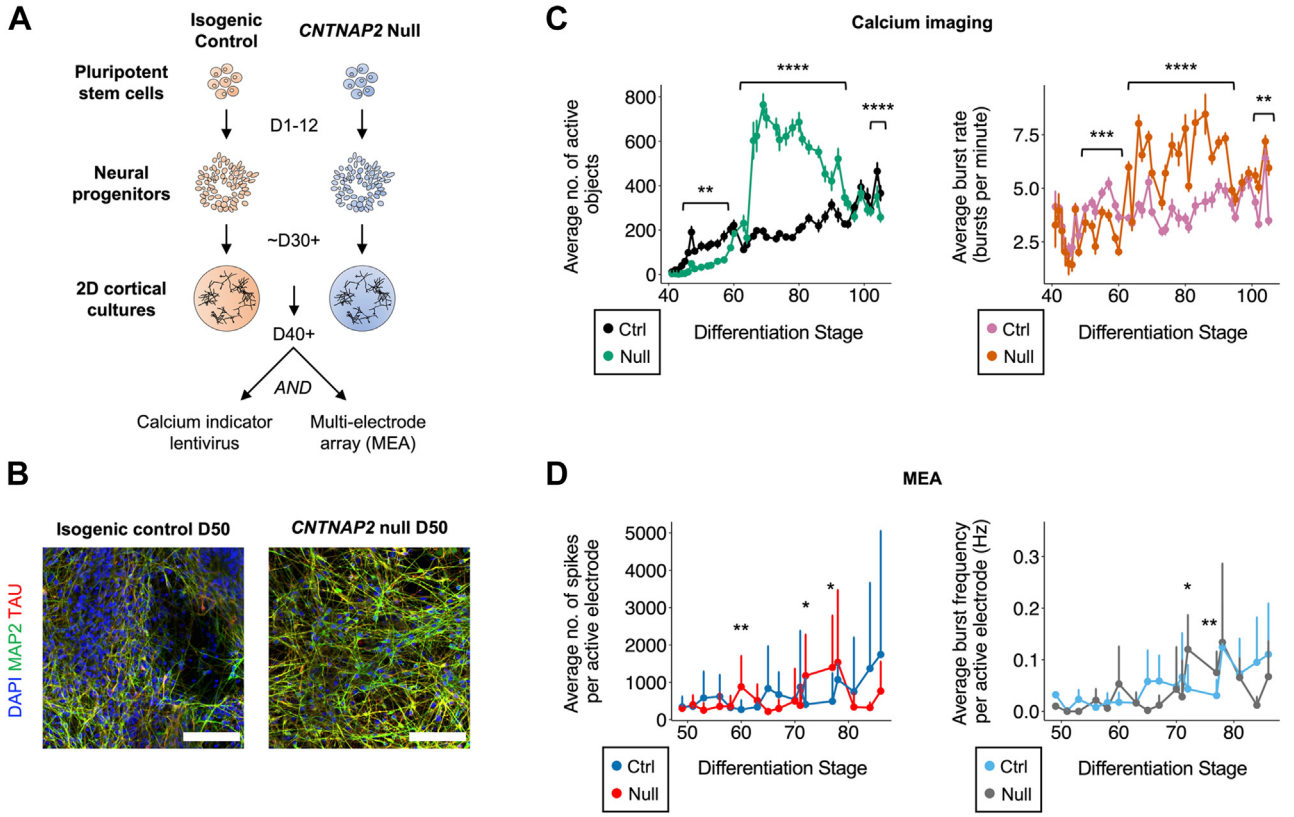

Figure 5. Loss of full-length *CNTNAP2* alters developing neural circuit activity. **(A)** Overview of the experimental setup to study network-level neuronal activity in induced pluripotent stem cells–derived *CNTNAP2* null and isogenic control cultures. To record activity, neuronal cultures were either infected with a lentiviral vector expressing a genetically encoded orange, fluorescent calcium indicator (mRuby based) or plated onto an MEA plate. Culture activity was then longitudinally measured by live calcium imaging or MEA over a course of ~30 to 60 days. **(B)** Cortical neurons are efficiently generated from *CNTNAP2* null induced pluripotent stem cells, as demonstrated by confocal imaging of immunostained D50 isogenic control and *CNTNAP2* null cortical differentiations for proteins localized to dendrites (MAP2, green), axons (tau, red), and cell bodies (nuclei labeled with $DAPI^+$, blue). Scale bar = 100 μm. **(C)** *CNTNAP2* null neurons and networks initially show lower activity than isogenic controls, as measured by calcium imaging. This is then followed by an extended (>30 days) period of significant hyperactivity in *CNTNAP2* null neurons. Activity was recorded every 24 to 48 hours and the average number of active neurons and average burst rate were calculated. Active objects are defined as cells or cell clusters that fire at least once over a 2-minute scan. From ~D60 to D90, the number of active objects and the average burst rate were significantly increased in *CNTNAP2* null neurons followed by a decrease in activity to a level equal to or below that of control cultures (Sidak's multiple comparisons test; $^{**}p < .01$, $^{***}p < .001$, $^{****}p < .0001$). Error bars show standard error, with each data point representing the average of 8 wells per genotype ($n = 2$ control inductions, 2 *CNTNAP2* null inductions). **(D)** Trends similar to those observed in the calcium imaging results were observed in the MEA experiments. D35 control and *CNTNAP2* null cortical cultures were plated on MEAs, and activity was recorded every 24 to 48 hours. *CNTNAP2* null cultures had significantly more spikes per active electrode at (D60, D72, and D77) and a higher burst frequency at D72 and D77 (pairwise *t* tests; $^{*}p < .05$, $^{**}p < .01$; $n = 1$ control induction, 1 *CNTNAP2* null induction). Both parameters then decreased in the null samples while continuing to increase in controls. Error bars show standard error. Ctrl, control; MEA, multielectrode array.

difference in activity between genotypes. Between ~D41 and D60, control neurons had a greater number of active objects and a higher burst rate (Sidak's multiple comparisons test; active objects: $p < .003$; burst rate: $p < .007$). From D63 onward, there was a marked switch in activity and a larger magnitude difference emerged, with null neurons being significantly more active than controls, both in terms of more active objects ($p < .0007$) and a higher burst rate ($p < .002$). Notably, while activity increased in control neurons at a relatively stable rate over weeks in culture, activity in *CNTNAP2* null neurons switched from increasing to decreasing from ~D70 onwards, eventually reducing to control levels.

Recording activity with MEAs revealed similar trends (Figure 5D) (two-way ANOVA; number of spikes: $F_{16,451} = 1.57$, $p = .07$; burst frequency: $F_{16,451} = 3.36$, $p < .0001$). Control neurons initially had more spikes and a higher burst frequency per active electrode than *CNTNAP2* null neurons until ~D60. Due to the high degree of variability in the MEA readings, however, these comparisons were not significant by post hoc analysis. From D60 until D77, null neurons recorded more spikes and a higher burst frequency per active electrode (Welch's *t* test; number of spikes: D60: $p = .004$; D72: $p = .03$; and D77: $p = .02$; burst frequency: D72: $p = .03$; D77: $p = .008$). Again, activity steadily increased throughout the experiment in control neurons but began to decrease from ~D80 in

CNTNAP2 null cultures, dropping below the level of controls by D81.

DISCUSSION

We report here that complete loss of function of the long isoform of *CNTNAP2* has multiple effects on cortical development. Comparing iPSCs null for full-length *CNTNAP2* with isogenic controls from the same donor cell line, we found that loss of *CNTNAP2* leads to specific defects in the generation and differentiation of the first-born neurons in the cortex. Furthermore, loss of *CNTNAP2* leads to cell autonomous defects in neurite outgrowth and branching, reducing excitatory neuron dendritic arbor complexity. Loss of *CNTNAP2* significantly alters cortical excitatory network function, manifesting in an initial period of reduced activity, a subsequent lengthy phase of developing network hyperexcitability, followed by a reduction in spontaneous activity below control network levels.

To study the consequences of loss of full-length *CNTNAP2* for human cortical development, we used scRNA-Seq to compare both cell composition and gene expression between *CNTNAP2* null and isogenic control human iPSC–derived cortical progenitors and neurons. Within cortical neurons, the most significantly differentially expressed genes included downregulation of *LMO3*, *CSRP2*, and *NEUROD2* in null neurons and upregulation of *CALB2* and *NTS*. This likely reflects changes in neuronal subpopulations—both in terms of gene expression and relative proportions. *CNTNAP2* null differentiations had a smaller proportion of cells in the *LMO3*$^+$/late 2 population (which highly expresses the downregulated genes) and a higher proportion in the *CALB2*$^+$/late 1 population (which highly expresses the upregulated genes). Unfortunately, with 2 independent scRNA-Seq experiments, there is not sufficient power to assign statistical significance to changes in cell proportions, whereas the experiments are powered to detect significant changes in gene expression.

While we were not able to conclusively say whether the *LMO3*$^+$/late 2 and *CALB2*$^+$/late 1 neurons are two distinct terminally differentiated neuronal populations, or whether one population is a transition stage to another, there is evidence suggesting that the *CALB2*$^+$/late 1 population may be precursors of the *LMO3*$^+$/late 2 group. By Carnegie stage 21, the human pioneer cortical plate contains primarily *CALB2*$^+$/*TBR1*$^+$ neurons (68). *CALB2*$^+$ pioneer neurons disappear shortly after the formation of the definitive cortical plate, which is established around Carnegie stage 21/22 when *TBR1*$^+$/*CALB2*-negative neurons appear.

In contrast, *LMO3* expression is almost entirely restricted in its onset of expression to the cortical subplate, which forms at a later developmental stage than the pioneer cortical plate (69). One possibility is that the *CALB2*$^+$/late 1 population are presubplate cells that subsequently downregulate *CALB2* and upregulate *LMO3*. This would suggest that the *CNTNAP2* null cells are delayed or retained in the *CALB2*-high stage, rather than progressing on to an *LMO3*-high stage. Alternatively, loss of *CNTNAP2* could lead to an increased production of *CALB2*$^+$ early neurons from cortical progenitor cells.

Additionally, we analyzed neurite development in both *CNTNAP2* null and isogenic control excitatory neurons. *CNTNAP2* null neurons exhibit defects in neurite outgrowth, with the number of branches per neuron reduced compared with controls. Analysis of *CNTNAP2* null neurons cocultured with isogenic control neurons demonstrated that the reduction in neurite branching is a cell autonomous phenotype. The reduction in branch number was also more significant in the cocultures. We believe that this is due to the coculture technique controlling for variability between extracellular environments. Such variability may have obscured some of the reduction in branching and/or neurite length in the single-genotype cultures.

Finally, in addition to neuronal morphogenesis, we also studied the effect of *CNTNAP2* LOF on excitatory neural network development, using calcium imaging and MEAs. Both approaches demonstrated that *CNTNAP2* null cortical networks were significantly more active than those of isogenic controls, beginning around D60, before reverting to control levels and eventually demonstrating reduced activity. The early hyperactivity phenotype is consistent with previous reports of human forebrain networks generated from iPSCs with a heterozygous *CNTNAP2* mutation (derived from an individual with schizophrenia) (70).

Recent work has suggested that *CNTNAP2* acts to promote calcium export from neurons, thereby suppressing excitability and network activity (71). A loss of *CNTNAP2* could therefore lead to hyperexcitability by increasing intracellular calcium, a hypothesis that should be tested in future experiments. Such a mechanism could also explain the reduction in neurite branching that we observed. Neurite outgrowth may be suppressed to compensate for the heightened activity of the null cells.

Altered neuronal activity has been reported in postnatal *Cntnap2* null mice, in which *Cntnap2* null neurons were hypoactive (47,48,72–74). Midgestation and prenatal cortical network activity in these models have not been reported; however, the reduced postnatal activity in mouse models is consistent with the late-stage phenotypes of reduced human cortical network activity reported here. Furthermore, while our model system does not produce cortical interneurons, there is robust evidence that alterations in GABAergic (gamma-aminobutyric acidergic) signaling also occur in the context of reduced *CNTNAP2* dosage (75,76). Further investigation into cortical interneuron dynamics in a human *CNTNAP2* null model should also be conducted.

We conclude that *CNTNAP2* LOF mutations change multiple aspects of cortical development, ranging from neuronal subtype differentiation to the formation of neural circuitry. Because these phenotypes affect the earliest born neurons, they are also likely to have lasting effects on the developing neonatal cortex. Because basic connectivity is established prenatally in most mammals, alterations to this scaffold could affect downstream steps of brain formation (77). Even transient changes have been shown to exert such an effect (78,79). Related to this, it would be important to assess whether the defects observed in our study could be rescued by overexpression of *CNTNAP2* and at what point in development, rescue is no longer possible. It will also be critical to supplement the experiments in this study with *CNTNAP2* null cultures derived from additional donor cell lines. Replicating our results in different genetic backgrounds will be a key next step.

These findings could have important implications for the diagnosis and treatment of *CNTNAP2*-related disorders. They may also provide important insights for neurodevelopmental disorders more generally, including those not directly involving *CNTNAP2*, but that may be underpinned by similar pathophysiological mechanisms.

ACKNOWLEDGMENTS AND DISCLOSURES

FJL's group is supported by a Wellcome Trust Senior Investigator Award WT101052MA, Great Ormond Street Children's Charity (Stem Cell Professorship), and Alzheimer's Research UK (Stem Cell Research Center). FSG-H was funded by the Canadian Centennial Scholarship Fund. This research was supported by the National Institute for Health and Care Research Great Ormond Street Biomedical Research Centre.

We thank Elsa Ghirardini, Steven Moore, and Tom Campbell for their assistance with the neurite outgrowth and neuronal activity assays. We also thank Vickie Stubbs and Ellie Tuck for performing cortical differentiations, Alessio Strano for designing the Nanostring panel, and all members of the Livesey Laboratory for their feedback throughout this project.

FJL is a founder and director of Talisman Therapeutics and of Gen2 Neuroscience, companies carrying out research and development for neurodegenerative diseases.

ARTICLE INFORMATION

From the University College London Great Ormond Street Institute of Child Health, Zayed Centre for Research into Rare Disease in Children, University College London, London, United Kingdom (FSG-H, MH, FJL); Estonian Biocentre, Institute of Genomics, University of Tartu, Tartu, Estonia (TK); and the Department of Human Genetics, KU Leuven, Leuven, Belgium (TK).

Address correspondence to Frederick J. Livesey, Mb.Ch.B., Ph.D., at r.livesey@ucl.ac.uk or rick@talisman-therapeutics.com.

Received Apr 22, 2022; revised Mar 10, 2023; accepted Mar 13, 2023.

Supplementary material cited in this article is available online at https://doi.org/10.1016/j.biopsych.2023.03.014.

REFERENCES

1. Moreno-De-Luca A, Myers SM, Challman TD, Moreno-De-Luca D, Evans DW, Ledbetter DH (2013): Developmental brain dysfunction: Revival and expansion of old concepts based on new genetic evidence [published correction appears in Lancet Neurol 2013;12:423]. Lancet Neurol 12:406–414.
2. De Rubeis S, He X, Goldberg AP, Poultney CS, Samocha K, Cicek AE, *et al.* (2014): Synaptic, transcriptional and chromatin genes disrupted in autism. Nature 515:209–215.
3. Bakkaloglu B, O'Roak BJ, Louvi A, Gupta AR, Abelson JF, Morgan TM, *et al.* (2008): Molecular cytogenetic analysis and resequencing of contactin associated protein-like 2 in autism spectrum disorders. Am J Hum Genet 82:165–173.
4. Arking DE, Cutler DJ, Brune CW, Teslovich TM, West K, Ikeda M, *et al.* (2008): A common genetic variant in the neurexin superfamily member CNTNAP2 increases familial risk of autism. Am J Hum Genet 82:160–164.
5. Alarcon M, Abrahams BS, Stone JL, Duvall JA, Perederiy JV, Bomar JM, *et al.* (2008): Linkage, association, and gene-expression analyses identify CNTNAP2 as an autism-susceptibility gene. Am J Hum Genet 82:150–159.
6. Rossi E, Verri AP, Patricelli MG, Destefani V, Ricca I, Vetro A, *et al.* (2008): A 12Mb deletion at 7q33-q35 associated with autism spectrum disorders and primary amenorrhea. Eur J Med Genet 51:631–638.
7. Li X, Hu Z, He Y, Xiong Z, Long Z, Peng Y, *et al.* (2010): Association analysis of CNTNAP2 polymorphisms with autism in the Chinese Han population. Psychiatr Genet 20:113–117.
8. Steer CD, Golding J, Bolton PF (2010): Traits contributing to the autistic spectrum. PLoS One 5:e12633.
9. Nord AS, Roeb W, Dickel DE, Walsh T, Kusenda M, O'Connor KL, *et al.* (2011): Reduced transcript expression of genes affected by inherited and de novo CNVs in autism. Eur J Hum Genet 19:727–731.
10. O'Roak BJ, Deriziotis P, Lee C, Vives L, Schwartz JJ, Girirajan S, *et al.* (2011): Exome sequencing in sporadic autism spectrum disorders identifies severe de novo mutations [published correction appears in Nat Genet 2012;44:471. Nat Genet 43:585–589.
11. Anney R, Klei L, Pinto D, Almeida J, Bacchelli E, Baird G, *et al.* (2012): Individual common variants exert weak effects on the risk for autism spectrum disorders. Hum Mol Genet 21:4781–4792.
12. Prasad A, Merico D, Thiruvahindrapuram B, Wei J, Lionel AC, Sato D, *et al.* (2012): A discovery resource of rare copy number variations in individuals with autism spectrum disorder. G3 (Bethesda) 2:1665–1685.
13. Sampath S, Bhat S, Gupta S, O'Connor A, West AB, Arking DE, Chakravarti A (2013): Defining the contribution of CNTNAP2 to autism susceptibility. PLoS One 8:e77906.
14. Girirajan S, Dennis MY, Baker C, Malig M, Coe BP, Campbell CD, *et al.* (2013): Refinement and discovery of new hotspots of copy-number variation associated with autism spectrum disorder. Am J Hum Genet 92:221–237.
15. Koshimizu E, Miyatake S, Okamoto N, Nakashima M, Tsurusaki Y, Miyake N, *et al.* (2013): Performance comparison of bench-top next generation sequencers using microdroplet PCR-based enrichment for targeted sequencing in patients with autism spectrum disorder. PLoS One 8:e74167.
16. Chiocchetti AG, Kopp M, Waltes R, Haslinger D, Duketis E, Jarczok TA, *et al.* (2015): Variants of the CNTNAP2 5′ promoter as risk factors for autism spectrum disorders: A genetic and functional approach. Mol Psychiatry 20:839–849.
17. Eriksson MA, Liedén A, Westerlund J, Bremer A, Wincent J, Sahlin E, *et al.* (2015): Rare copy number variants are common in young children with autism spectrum disorder. Acta Paediatr 104:610–618.
18. Nascimento PP, Bossolani-Martins AL, Rosan DB, Mattos LC, Brandão-Mattos C, Fett-Conte AC (2016): Single nucleotide polymorphisms in the CNTNAP2 gene in Brazilian patients with autistic spectrum disorder. Genet Mol Res 15(1).
19. Zhou WZ, Zhang J, Li Z, Lin X, Li J, Wang S, *et al.* (2019): Targeted resequencing of 358 candidate genes for autism spectrum disorder in a Chinese cohort reveals diagnostic potential and genotype-phenotype correlations. Hum Mutat 40:801–815.
20. Aspromonte MC, Bellini M, Gasparini A, Carraro M, Bettella E, Polli R, *et al.* (2019): Characterization of intellectual disability and autism comorbidity through gene panel sequencing [published correction appears in Hum Mutat 2020;41:1183]. Hum Mutat 40:1346–1363.
21. Egger G, Roetzer KM, Noor A, Lionel AC, Mahmood H, Schwarzbraun T, *et al.* (2014): Identification of risk genes for autism spectrum disorder through copy number variation analysis in Austrian families. Neurogenetics 15:117–127.
22. Belloso JM, Bache I, Guitart M, Caballin MR, Halgren C, Kirchhoff M, *et al.* (2007): Disruption of the CNTNAP2 gene in a t(7;15) translocation family without symptoms of Gilles de la Tourette syndrome. Eur J Hum Genet 15:711–713.
23. Watson CM, Crinnion LA, Tzika A, Mills A, Coates A, Pendlebury M, *et al.* (2014): Diagnostic whole genome sequencing and split-read mapping for nucleotide resolution breakpoint identification in CNTNAP2 deficiency syndrome. Am J Med Genet A 164A:2649–2655.
24. Karaca E, Harel T, Pehlivan D, Jhangiani SN, Gambin T, Akdemir CZ, *et al.* (2015): Genes that affect brain structure and function identified by rare variant analyses of Mendelian neurologic disease. Neuron 88:499–513.
25. Smogavec M, Cleall A, Hoyer J, Lederer D, Nassogne MC, Palmer EE, *et al.* (2016): Eight further individuals with intellectual disability and epilepsy carrying bi-allelic CNTNAP2 aberrations allow delineation of the mutational and phenotypic spectrum. J Med Genet 53:820–827.
26. Vernes SC, Newbury DF, Abrahams BS, Winchester L, Nicod J, Groszer M, *et al.* (2008): A functional genetic link between distinct developmental language disorders. N Engl J Med 359:2337–2345.

27. Petrin AL, Giacheti CM, Maximino LP, Abramides DV, Zanchetta S, Rossi NF, *et al.* (2010): Identification of a microdeletion at the 7q33-q35 disrupting the CNTNAP2 gene in a Brazilian stuttering case. Am J Med Genet A 152A:3164–3172.
28. Newbury DF, Paracchini S, Scerri TS, Winchester L, Addis L, Richardson AJ, *et al.* (2011): Investigation of dyslexia and SLI risk variants in reading- and language-impaired subjects. Behav Genet 41:90–104.
29. Stein MB, Yang BZ, Chavira DA, Hitchcock CA, Sung SC, Shipon-Blum E, Gelernter J (2011): A common genetic variant in the neurexin superfamily member CNTNAP2 is associated with increased risk for selective mutism and social anxiety-related traits. Biol Psychiatry 69:825–831.
30. Al-Murrani A, Ashton F, Aftimos S, George AM, Love DR (2012): Amino-terminal microdeletion within the CNTNAP2 gene associated with variable expressivity of speech delay. Case Rep Genet 2012: 172408.
31. Laffin JJ, Raca G, Jackson CA, Strand EA, Jakielski KJ, Shriberg LD (2012): Novel candidate genes and regions for childhood apraxia of speech identified by array comparative genomic hybridization [published correction appears in Genet Med 2013;15:587–588]. Genet Med 14:928–936.
32. Centanni TM, Sanmann JN, Green JR, Iuzzini-Seigel J, Bartlett C, Sanger WG, Hogan TP (2015): The role of candidate-gene CNTNAP2 in childhood apraxia of speech and specific language impairment. Am J Med Genet B Neuropsychiatr Genet 168:536–543.
33. Chen XS, Reader RH, Hoischen A, Veltman JA, Simpson NH, Francks C, *et al.* (2017): Next-generation DNA sequencing identifies novel gene variants and pathways involved in specific language impairment. Sci Rep 7:46105.
34. Mefford HC, Muhle H, Ostertag P, von Spiczak S, Buysse K, Baker C, *et al.* (2010): Genome-wide copy number variation in epilepsy: Novel susceptibility loci in idiopathic generalized and focal epilepsies. PLoS Genet 6:e1000962.
35. Lesca G, Rudolf G, Labalme A, Hirsch E, Arzimanoglou A, Genton P, *et al.* (2012): Epileptic encephalopathies of the Landau-Kleffner and continuous spike and waves during slow-wave sleep types: Genomic dissection makes the link with autism. Epilepsia 53:1526–1538.
36. Pippucci T, Licchetta L, Baldassari S, Palombo F, Menghi V, D'Aurizio R, *et al.* (2015): Epilepsy with auditory features: A heterogeneous clinico-molecular disease. Neurol Genet 1:e5.
37. Strauss KA, Puffenberger EG, Huentelman MJ, Gottlieb S, Dobrin SE, Parod JM, *et al.* (2006): Recessive symptomatic focal epilepsy and mutant contactin-associated protein-like 2. N Engl J Med 354:1370–1377.
38. Rodenas-Cuadrado P, Ho J, Vernes SC (2014): Shining a light on CNTNAP2: Complex functions to complex disorders. Eur J Hum Genet 22:171–178.
39. Velmeshev D, Schirmer L, Jung D, Haeussler M, Perez Y, Mayer S, *et al.* (2019): Single-cell genomics identifies cell type-specific molecular changes in autism. Science 364:685–689.
40. Poliak S, Gollan L, Martinez R, Custer A, Einheber S, Salzer JL, *et al.* (1999): Caspr2, a new member of the neurexin superfamily, is localized at the juxtaparanodes of myelinated axons and associates with K+ channels. Neuron 24:1037–1047.
41. Betancur C, Sakurai T, Buxbaum JD (2009): The emerging role of synaptic cell-adhesion pathways in the pathogenesis of autism spectrum disorders. Trends Neurosci 32:402–412.
42. Poliak S, Salomon D, Elhanany H, Sabanay H, Kiernan B, Pevny L, *et al.* (2003): Juxtaparanodal clustering of Shaker-like K+ channels in myelinated axons depends on Caspr2 and TAG-1. J Cell Biol 162:1149–1160.
43. Anderson GR, Galfin T, Xu W, Aoto J, Malenka RC, Südhof TC (2012): Candidate autism gene screen identifies critical role for cell-adhesion molecule CASPR2 in dendritic arborization and spine development. Proc Natl Acad Sci U S A 109:18120–18125.
44. Canali G, Garcia M, Hivert B, Pinatel D, Goullancourt A, Oguievetskaia K, *et al.* (2018): Genetic variants in autism-related CNTNAP2 impair axonal growth of cortical neurons. Hum Mol Genet 27:1941–1954.
45. Gao R, Piguel NH, Melendez-Zaidi AE, Martin-de-Saavedra MD, Yoon S, Forrest MP, *et al.* (2018): CNTNAP2 stabilizes interneuron dendritic arbors through CASK. Mol Psychiatry 23:1832–1850.
46. Gdalyahu A, Lazaro M, Penagarikano O, Golshani P, Trachtenberg JT, Geschwind DH (2015): The autism related protein contactin-associated protein-like 2 (CNTNAP2) stabilizes new spines: An in vivo mouse study [published correction appears in PLoS One 2015;10:e0129638. Gescwind, Daniel H [corrected to Geschwind, Daniel H]]. PLoS One 10:e0125633.
47. Lazaro MT, Taxidis J, Shuman T, Bachmutsky I, Ikrar T, Santos R, *et al.* (2019): Reduced prefrontal synaptic connectivity and disturbed oscillatory population dynamics in the CNTNAP2 model of autism. Cell Rep 27:2567–2578.e6.
48. Varea O, Martin-de-Saavedra MD, Kopeikina KJ, Schurmann B, Fleming HJ, Fawcett-Patel JM, *et al.* (2015): Synaptic abnormalities and cytoplasmic glutamate receptor aggregates in contactin associated protein-like 2/Caspr2 knockout neurons. Proc Natl Acad Sci U S A 112:6176–6181.
49. Shi Y, Kirwan P, Livesey FJ (2012): Directed differentiation of human pluripotent stem cells to cerebral cortex neurons and neural networks. Nat Protoc 7:1836–1846.
50. Shi Y, Kirwan P, Smith J, Robinson HP, Livesey FJ (2012): Human cerebral cortex development from pluripotent stem cells to functional excitatory synapses. Nat Neurosci 15:477–486.. S1.
51. Israel MA, Yuan SH, Bardy C, Reyna SM, Mu Y, Herrera C, *et al.* (2012): Probing sporadic and familial Alzheimer's disease using induced pluripotent stem cells. Nature 482:216–220.
52. Bruntraeger M, Byrne M, Long K, Bassett AR (2019): Editing the genome of human induced pluripotent stem cells using CRISPR/Cas9 ribonucleoprotein complexes. Methods Mol Biol 1961:153–183.
53. Stoeckius M, Zheng S, Houck-Loomis B, Hao S, Yeung BZ, Mauck WM 3rd, *et al.* (2018): Cell hashing with barcoded antibodies enables multiplexing and doublet detection for single cell genomics. Genome Biol 19:224.
54. Love MI, Huber W, Anders S (2014): Moderated estimation of fold change and dispersion for RNA-seq data with DESeq2. Genome Biol 15:550.
55. Rodriguez A, Ehlenberger DB, Dickstein DL, Hof PR, Wearne SL (2008): Automated three-dimensional detection and shape classification of dendritic spines from fluorescence microscopy images. PLoS One 3:e1997.
56. Strano A, Tuck E, Stubbs VE, Livesey FJ (2020): Variable outcomes in neural differentiation of human PSCs arise from intrinsic differences in developmental signaling pathways. Cell Rep 31:107732.
57. Kirwan P, Turner-Bridger B, Peter M, Momoh A, Arambepola D, Robinson HP, Livesey FJ (2015): Development and function of human cerebral cortex neural networks from pluripotent stem cells in vitro. Development 142:3178–3187.
58. Lee IS, Carvalho CM, Douvaras P, Ho SM, Hartley BJ, Zuccherato LW, *et al.* (2015): Characterization of molecular and cellular phenotypes associated with a heterozygous CNTNAP2 deletion using patient-derived hiPSC neural cells. NPJ Schizophr 1:15019.
59. Zhang P, Dimont E, Ha T, Swanson DJ, , FANTOM Consortium, Hide W, Goldowitz D (2017): Relatively frequent switching of transcription start sites during cerebellar development [published correction appears in BMC Genomics 2018;19:39]. BMC Genomics 18:461.
60. Burke EE, Chenoweth JG, Shin JH, Collado-Torres L, Kim SK, Micali N, *et al.* (2020): Dissecting transcriptomic signatures of neuronal differentiation and maturation using iPSCs. Nat Commun 11:462.
61. Poot M (2015): Connecting the CNTNAP2 networks with neurodevelopmental disorders. Mol Syndromol 6:7–22.
62. Miller JA, Ding SL, Sunkin SM, Smith KA, Ng L, Szafer A, *et al.* (2014): Transcriptional landscape of the prenatal human brain. Nature 508:199–206.

63. Nowakowski TJ, Pollen AA, Sandoval-Espinosa C, Kriegstein AR (2016): Transformation of the radial glia scaffold demarcates two stages of human cerebral cortex development. Neuron 91:1219–1227.
64. Cadwell CR, Bhaduri A, Mostajo-Radji MA, Keefe MG, Nowakowski TJ (2019): Development and arealization of the cerebral cortex. Neuron 103:980–1004.
65. Roadmap Epigenomics Consortium, Kundaje A, Meuleman W, Ernst J, Bilenky M, Yen A, *et al.* (2015): Integrative analysis of 111 reference human epigenomes. Nature 518:317–330.
66. Street K, Risso D, Fletcher RB, Das D, Ngai J, Yosef N, *et al.* (2018): Slingshot: Cell lineage and pseudotime inference for single-cell transcriptomics. BMC Genomics 19:477.
67. Camp JG, Badsha F, Florio M, Kanton S, Gerber T, Wilsch-Bräuninger M, *et al.* (2015): Human cerebral organoids recapitulate gene expression programs of fetal neocortex development. Proc Natl Acad Sci U S A 112:15672.
68. González-Gómez M, Meyer G (2014): Dynamic expression of calretinin in embryonic and early fetal human cortex. Front Neuroanat 8:41.
69. Ozair MZ, Kirst C, van den Berg BL, Ruzo A, Rito T, Brivanlou AH (2018): hPSC modeling reveals that fate selection of cortical deep projection neurons occurs in the subplate. Cell Stem Cell 23:60–73.e6.
70. Flaherty E, Deranieh RM, Artimovich E, Lee IS, Siegel AJ, Levy DL, *et al.* (2017): Patient-derived hiPSC neurons with heterozygous CNTNAP2 deletions display altered neuronal gene expression and network activity. NPJ Schizophr 3:35.
71. Martín-de-Saavedra MD, Dos Santos M, Culotta L, Varea O, Spielman BP, Parnell E, *et al.* (2022): Shed CNTNAP2 ectodomain is detectable in CSF and regulates Ca^{2+} homeostasis and network synchrony via PMCA2/ATP2B2. Neuron 110:627–643.e9.
72. Scott-Van Zeeland AA, Abrahams BS, Alvarez-Retuerto AI, Sonnenblick LI, Rudie JD, Ghahremani D, *et al.* (2010): Altered functional connectivity in frontal lobe circuits is associated with variation in the autism risk gene CNTNAP2. Sci Transl Med 2:56ra80.
73. Kim JW, Park K, Kang RJ, Gonzales ELT, Kim DG, Oh HA, *et al.* (2019): Pharmacological modulation of AMPA receptor rescues social impairments in animal models of autism. Neuropsychopharmacology 44:314–323.
74. Antoine MW, Langberg T, Schnepel P, Feldman DE (2019): Increased excitation-inhibition ratio stabilizes synapse and circuit excitability in four autism mouse models. Neuron 101:648–661.e4.
75. Gao R, Zaccard CR, Shapiro LP, Dionisio LE, Martin-de-Saavedra MD, Piguel NH, *et al.* (2019): The CNTNAP2-CASK complex modulates GluA1 subcellular distribution in interneurons. Neurosci Lett 701:92–99.
76. Hali S, Kim J, Kwak TH, Lee H, Shin CY, Han DW (2020): Modelling monogenic autism spectrum disorder using mouse cortical organoids. Biochem Biophys Res Commun 521:164–171.
77. Levitt P (2003): Structural and functional maturation of the developing primate brain. J Pediatr 143:S35–S45.
78. Mirabella F, Desiato G, Mancinelli S, Fossati G, Rasile M, Morini R, *et al.* (2021): Prenatal interleukin 6 elevation increases glutamatergic synapse density and disrupts hippocampal connectivity in offspring. Immunity 54:2611–2631.e8.
79. Sretavan DW, Shatz CJ, Stryker MP (1988): Modification of retinal ganglion cell axon morphology by prenatal infusion of tetrodotoxin. Nature 336:468–471.